Covalent bonding and band-gap formation in ternary transition-metal di-aluminides: Al_4MnCo and related compounds

2002 J. Phys.: Condens. Matter 14 7201

(http://iopscience.iop.org/0953-8984/14/30/310)

INSTITUTE OF PHYSICS PUBLISHING JOURNAL OF PHYSICS: CONDENSED MATTER

J. Phys.: Condens. Matter **14** (2002) 7201–7219 PII: S0953-8984(02)36548-2

Covalent bonding and band-gap formation in ternary transition-metal di-aluminides: Al_4MnCo and related compounds

M Krajčí[1,2,3] **and J Hafner**[1]

[1] Institut für Materialphysik and Centre for Computational Materials Science, Universität Wien, Sensengasse 8/12, A-1090 Wien, Austria
[2] Institute of Physics, Slovak Academy of Sciences, Dúbravská cesta 9, SK 84228 Bratislava, Slovakia

E-mail: fyzikraj@savba.sk

Received 2 May 2002, in final form 18 June 2002
Published 17 July 2002
Online at stacks.iop.org/JPhysCM/14/7201

Abstract

In this paper we extend our previous study of the electronic structure of and bonding mechanism in transition-metal (TM) di-aluminides to ternary systems. We have studied the character of the bonding in Al_4MnCo and related TM di-aluminides in the $C11_b$ ($MoSi_2$) and C54 ($TiSi_2$) crystal structures. A peculiar feature of the electronic structure of these TM di-aluminides is the existence of a semiconducting gap at the Fermi level. In our previous work we predicted a gap in Al_2TM compounds where the TM atoms have eight valence electrons. Here we demonstrate that the semiconducting gap does not disappear if the TM sites are occupied by two different TMs, provided that the electron-per-atom ratio is conserved. Such a replacement substantially increases the class of possibly semiconducting TM di-aluminides. Substitution for 3d TMs of 4d or 5d TMs enhances the width of the gap. From the analysis of the charge density distribution and the crystal orbital overlap population, we conclude that the bonding between atoms has dominantly covalent character. This is confirmed not only by the enhanced charge density halfway between atoms, but also by the clear bonding–antibonding splitting of the electronic states. If the gaps between split states that correspond to all bonding configurations in the crystal have a common overlap at the Fermi level, the intermetallic compound becomes a semiconductor. However, the results of the total-energy calculations suggest that the existence of a band gap does not necessarily imply a stable structure. Strong covalent bonds can exist also in Al–TM structures where no band gap is observed.

[3] Author to whom any correspondence should be addressed.

1. Introduction

Besides their well known technological importance, transition-metal (TM) aluminides also exhibit highly interesting and unexpected physical properties. Al-based compounds of TMs (e.g. the nanocrystalline phase $Al_{94}V_4Fe_2$) are among the most promising candidates for high-performance structural material applications [1]. The reported tensile strength above 1000 MPa exceeds the strength of usual technical steels. Aluminides form also an important class of quasicrystals, with exotic physical and chemical properties [2]. For instance, an icosahedral AlPdRe phase with a stoichiometric composition around $Al_{70.5}Pd_{21}Re_{8.5}$ exhibits anomalously high electrical resistivity. The absolute values of the reported resistivities may be as high as those of doped semiconductors, $\sim 1\ \Omega^{-1}\ \mathrm{cm}^{-1}$. The possibility of a metal–insulator transition in this system is currently an issue of great controversy [3, 4]. Alloys composed of metallic elements are naturally expected to be metallic too. However, some crystalline TM aluminides such as $RuAl_2$ were found to be semiconducting. The anomalous physical properties of TM aluminides are observed mostly in specific crystalline structures. The TM di-silicides $TMSi_2$ ($TiSi_2$, $CrSi_2$, $MoSi_2$) are one such family of structures. The $RuAl_2$ compound belongs to this class. A semiconducting behaviour has been reported also for TM aluminides in the BiF_3 structure [5]. The electronic structures of $RuAl_2$ and related compounds have been studied also by other authors [5–8].

Very recently [9] we have studied the character of the bonding in the Al_2Fe and related TM di-aluminides in three $TMSi_2$ crystal structures: $C11_b$ ($MoSi_2$), C40 ($CrSi_2$), and C54 ($TiSi_2$). A peculiar feature of the electronic structure of these TM di-aluminides is the existence of a gap at the Fermi level. The gap exists in all Al_2TM compounds where the TM atoms have eight valence electrons. We have found that a replacement of the 3d TMs by 4d or 5d TMs enhances the width of the gap. The gap exists also in Al_2TM compounds of the group VII and IX elements, but in this case the Fermi level is located above or below the gap. We studied the interatomic bonding by investigating the charge density distribution and by calculating the crystal orbital overlap population (COOP) [10] for selected configurations of atoms. Covalent bonds between the TM and Al atoms were identified from an enhanced charge density along the connections between the atoms. The COOP calculated for configurations of symmetrized orbitals revealed a bonding–antibonding splitting of the orbitals, confirming thus the covalent character of the bonds.

In the present paper we extend the investigations to ternary systems with two TMs. We demonstrate that the semiconducting gap that exists in the Al_2TM systems for a certain electron-per-atom ratio ($\approx$4.67) does not disappear if TM sites are occupied by two different TMs, TM_1 and TM_2, provided that the electron-per-atom ratio is conserved. Such replacements substantially increase the class of possibly semiconducting TM di-aluminides.

The composition of the system studied in the present paper is thus $Al_2(TM_1TM_2)$, or in a simpler notation $Al_4TM_1TM_2$. We shall restrict our study, similarly to in our previous paper, to the C54 and $C11_b$ crystal structures. As the primitive cell of these structures consists of two formula units, it is possible to replace two group VIII TM atoms with eight valence electrons by two different TM atoms, TM_1 and TM_2, with $8-i$ and $8+i$, $i = 1, 2, 3$, electrons, respectively. We restrict our study to the occupation of the TM sites by TM atoms from the same row of the periodic table. The C40 structure also belongs to the same family of layered structures as the $C11_b$ and C54 structures. However, as the primitive cell of the C40 structure consists of three formula units, a substitution conserving the electron-per-atom ratio would be possible only in a doubled cell. Because of the layered character of the $C11_b$ and C54 compounds, several variants for occupation of the layers by TM_1 or TM_2 atoms are possible. The calculation of the total energy will help to determine the most stable configuration.

Our paper is organized as follows: in section 2 we recapitulate briefly the structural characteristics of the studied systems. The calculated densities of states of nine $Al_4TM_1TM_2$ compounds in the C54 structure are presented in section 3. A detailed picture of the electronic structures of selected representative systems, namely Al_4MnCo and Al_4ReIr compounds, is discussed in section 3.1. Charge density distributions of Al_4MnCo in the $C11_b$ and C54 structures are studied in section 4. The results for the COOP calculated for configurations of symmetrized orbitals directed along the suspected bonds are presented in section 5. Section 6 summarizes our results and evaluates their significance for the current discussion of physical properties of TM–aluminium compounds.

2. Crystal structure

We have studied the properties of TM di-aluminides with the structure of TM di-silicides, i.e. the C54 ($TiSi_2$) and $C11_b$ ($MoSi_2$) crystal structures. The structures can be generated as different stacking sequences of the same pseudohexagonal TM–Al_2 layers [9, 11].

2.1. C54 ($TiSi_2$) crystal structure

Our ternary $Al_4TM_1TM_2$ structure is derived from the C54 structure by replacing the TM atom by either a TM_1 or a TM_2 atom. We investigated two possibilities for such a replacement. In the first one the occupation of the TM–Al_2 layers by TM_1 and TM_2 atoms is alternating. The TM_1 atoms occupy e.g. the A and C layers and the TM_2 the B and D layers in the ABCD sequence of layers. Because of the lack of a systematic nomenclature for such complex structures, we shall denote this structural variant as C54A. In the second possibility each layer has a mixed occupation of TM_1 and TM_2 atoms. In our nomenclature we shall denote this structure as C54M. From the total-energy calculations, we shall see in section 3.1.1 that the C54A structure is preferred.

2.2. $C11_b$ ($MoSi_2$) crystal structure

In the $C11_b$ structure the tetragonal symmetry allows only one possibility for occupation of the TM sites by two different TM_1 and TM_2 atoms: TM_1 atoms occupy TM sites in the (001) plane and TM_2 atoms occupy TM sites in the (002) plane. In our nomenclature we denote this structural variant as $C11_bM$. There is also a possibility of alternating TM_1–Al_2 and TM_2–Al_2 layers, similarly to in the case of C54 structure. TM_1 atoms occupy the A layer and TM_2 the B layer in the AB sequence of pseudohexagonal layers. However, such occupation breaks the space symmetry and reduces the tetragonal symmetry to the orthorhombic one. Our notation for this structure is $C11_bA$.

3. Density of states of ternary transition-metal di-aluminides

The electronic structure calculations have been performed using two different techniques: the plane-wave-based Vienna *ab initio* simulation package VASP [12, 13] has been used for the calculations of the electronic ground state and for the optimization of the atomic coordinates, volume, and geometry of the unit cell for all structures investigated. For each structure, forces and the stress tensor have been calculated and the positions of all atoms in the cell, and the lattice constants, have been optimized. The structural relaxation has a significant effect on the resulting electronic structure and gap formation. For instance, the width of the band gap at

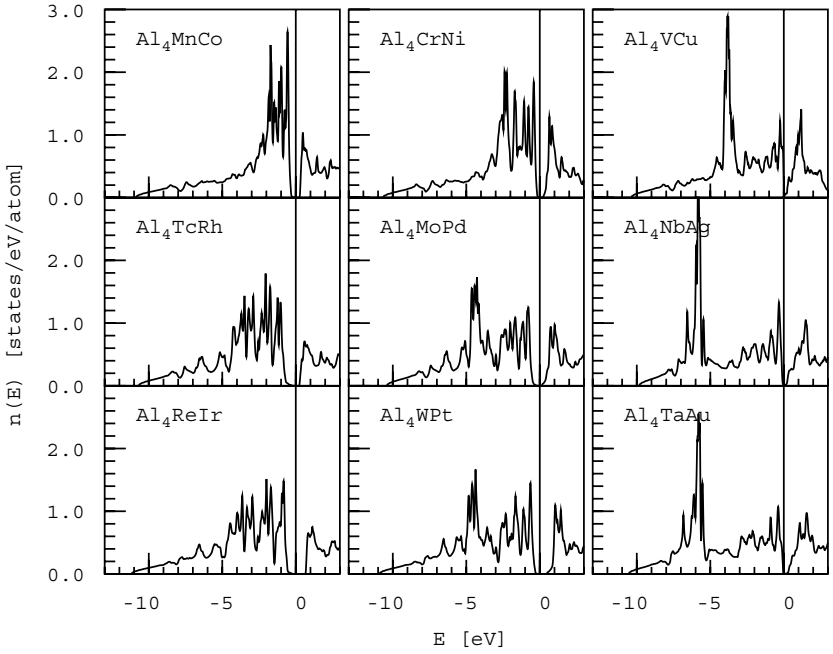

Figure 1. The total DOS of three 3d compounds of composition Al_4MnCo, Al_4CrNi, Al_4VCu, three 4d compounds of composition Al_4TcRh, Al_4MoPd, Al_4NbAg, and three 5d compounds of composition Al_4ReIr, Al_4WPt, Al_4TaAu. All the results relate to the C54A structure. The most interesting common feature of the DOSs of these compounds is the existence of a semiconducting band gap at the Fermi level.

the Fermi level for the Al_4MnCo compound in the C54 structure increased from 0.15 eV for a nonrelaxed lattice to 0.51 eV for the fully relaxed one.

However, a plane-wave-based approach such as that used in VASP produces only the Bloch states and the total density of states (DOS), a decomposition into local orbitals and local orbital-projected DOSs requiring additional assumptions. To achieve this decomposition, self-consistent electronic structure calculations have been performed using the tight-binding linear muffin-tin orbital (TB-LMTO) method [14–16] in an atomic-sphere approximation (ASA). The LMTO basis includes s, p, and d orbitals for each Al and TM atoms.

Figure 1 displays the total DOS of three 3d compounds of composition Al_4MnCo, Al_4CrNi, Al_4VCu, three 4d compounds of composition Al_4TcRh, Al_4MoPd, Al_4NbAg, and three 5d compounds of composition Al_4ReIr, Al_4WPt, Al_4TaAu. All the results relate to the C54 structure. The electronic structures were calculated for fully relaxed and optimized crystal structures. The structural parameters for all compounds investigated are listed in table 1.

The most significant common feature of the DOSs of these compounds is existence of a semiconducting band gap at the Fermi level. Comparison of the present results with the DOSs of group VIII TM di-aluminides, Al_2TM, TM = Fe, Ru, Os, studied in our previous paper [9] shows that if a TM of group VIII is replaced by two TMs from groups VII and IX, the band gap becomes even broader. The band gap of Al_4MnCo in the C54A structure is $E_g = 0.51$ eV, while the value for Al_2Fe in the C54 structure is $E_g = 0.41$ eV. However, if both TMs TM_1 and TM_2 are further from each other in the same row of the periodic table, the band gap narrows. The width of the gap in Al_4VCu shrinks to zero, leaving only a deep pseudogap at the Fermi level.

Table 1. Equilibrium lattice parameters a, b/a, and c/a, volume of the cell Ω, excess volume $\Delta\Omega$, total energy E_{tot}, heat of formation ΔH, and width of the gap at the Fermi level E_g for $Al_4TM_1TM_2$ in the C54A structure.

$Al_4TM_1TM_2$	a (Å)	b/a	c/a	Ω (Å^3/atom)	$\Delta\Omega$ (%)	E_{tot} (eV/atom)	ΔH (eV/atom)	E_g (eV)
Al_4MnCo	7.835	0.595	1.0954	13.075	−10.1	−5.4728	−0.399	0.511/0.290
Al_4TcRh	8.125	0.588	1.0905	14.341	−9.2	−6.0809	−0.723	0.586/0.302
Al_4ReIr	8.154	0.583	1.0920	14.373	−9.8	−6.5924	−0.627	1.019/0.698
Al_4CrNi	7.969	0.596	1.0865	13.665	−7.4	−5.2148	−0.279	0.450/0.215
Al_4MoPd	8.282	0.591	1.0829	15.146	−6.4	−5.6412	−0.510	0.466/0.174
Al_4WPt	8.299	0.586	1.0837	15.120	−7.2	−6.0946	−0.489	0.809/0.521
Al_4VCu	8.187	0.597	1.0823	14.783	−2.8	−4.6981	−0.122	0.000/0.000
Al_4NbAg	8.546	0.594	1.0785	16.675	−1.7	−4.7749	−0.167	0.165/0.000
Al_4TaAu	8.526	0.590	1.0778	16.445	−3.4	−5.1797	−0.221	0.276/0.053

The origin of the band gap lies in a special bonding of the d orbitals of the TM atoms with aluminium s, p orbitals. It is remarkable that the (pseudo)gap is clearly seen even for the Al_4VCu. As the compound contains early and late TMs, the centres of the d bands are rather well separated and far from the region of strongest hybridization which apparently extends around the Fermi level.

The present results confirm the trend reported already in our previous study [9] of the replacement of 3d TMs by 4d and 5d metals resulting in a broader gap. The broadest gap is observed for the Al_4ReIr compound. Although its width is reduced by a tail extending from lower energies, the value $E_g = 0.7$ eV is comparable with that of the band gap of germanium ($E_g = 0.74$ eV). The widths of the band gaps E_g for all compounds investigated are listed together with the structural and other parameters in table 1.

In the next section we shall continue with a detailed analysis of the electronic structure of a selected compound—Al_4MnCo. One can consider the electronic structure of this compound as representative also for other compounds. To demonstrate the similarities of the significant features of the electronic structures, we present also some results for the Al_4ReIr compound.

3.1. Electronic density of states of Al_4MnCo

3.1.1. The C54 structure. Al_4MnCo is derived from the Al_2Fe in the C54 structure, where Mn and Co atoms replace Fe sites. First we consider the structural variant with alternating Mn–Al_2 and Co–Al_2 layers. Figure 2 shows the DOS of Al_4MnCo in the C54A structure. The figure presents the total DOS (a), the partial aluminium DOS (b), partial TM DOSs for Mn (c) and Co (d) atoms. The thin line indicates the contribution from d states. One can see that the partial Mn and Co DOSs have almost uniquely d character. The partial Al DOS is dominated by s and p orbitals, but the contribution from d states at energies around E_F is not negligible.

The electronic structure of Al_4MnCo is in its most important features similar to that of Al_2Fe [9]. As already stressed, the most interesting feature is the gap at Fermi level. Its width is reduced by a tail of the DOS extending from lower energies. The partial aluminium DOS (see figure 2(b)) shows that the tail has dominantly Al character. Because of this tail, the definition of the band gap is not easy. Similarly to in the Al_2Fe or Al_2Ru compounds, the valence band maximum is found in an isolated band with strong dispersion [8, 9]; hence the sharp drop in the valence band DOS is followed by a very flat tail extending to higher energies. To cope with this situation, the width E_g of the gap is described by two numbers. The first

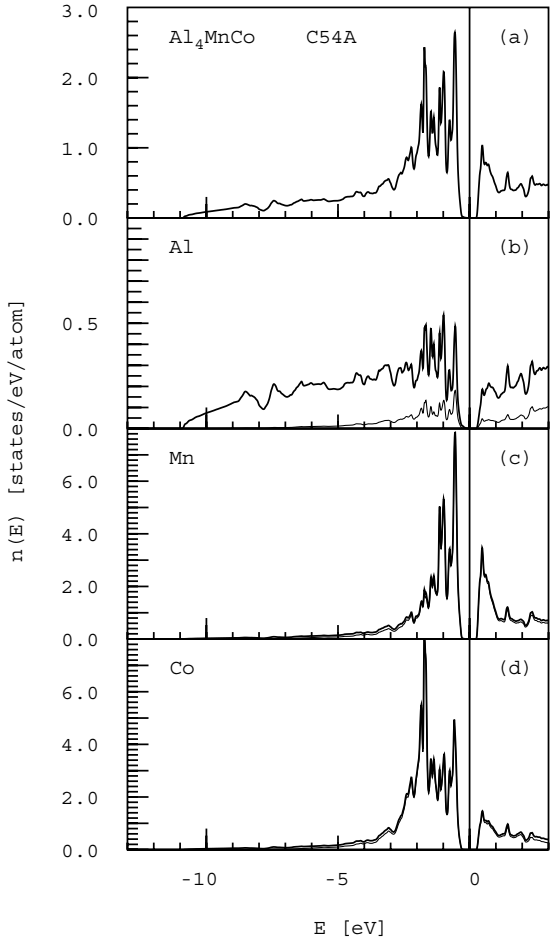

Figure 2. The DOS of Al_4MnCo in the C54A structure. The figure presents the total DOS (a), the partial aluminium DOS (b), partial TM DOSs for Mn (c) and Co (d) atoms. The thin line indicates the d-state contribution.

number gives the width of the energy interval where the integrated density states is equal to the total number of electrons in the system with accuracy better than 0.01 electrons. The second number gives the width of the energy interval where the total density of states is zero with a numerical accuracy better than 10^{-4} states eV^{-1}/atom. For further discussion we shall use the former definition.

The bandwidth measured from the bottom of the band is $W = 10.9$ eV. This value is comparable to that of pure fcc Al where $W = 11.4$ eV. The bandwidth W is a quantity sensitive to the interatomic distances and the equilibrium volume of the cell. It is remarkable that the equilibrium volume of the unit cell resulting from the structural relaxation is significantly lower than that expected according to Vegard's law.

The equilibrium volume calculated by VASP for Al_4MnCo in the C54A structure is 13.076 Å^3, a value substantially lower than the value 14.544 Å^3 predicted from the equilibrium volumes of fcc Al (16.490 Å^3), hcp Mn (10.780 Å^3), and hcp Co (10.450 Å^3) by Vegard's law. Equilibrium volumes and relative excess volumes for all structures

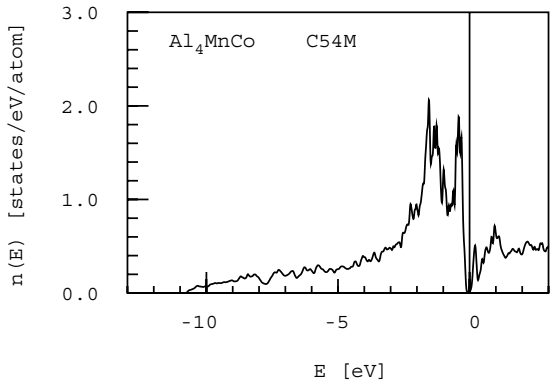

Figure 3. The DOS of the Al_4MnCo in the C54M structure with mixed occupation of pseudohexagonal layers.

Table 2. Equilibrium volume Ω, excess volume $\Delta\Omega$, total energy E_{tot}, heat of formation ΔH, and width of the gap at the Fermi level E_g of Al_4MnCo for several lattice types.

Al_4MnCo in lattice	Ω (Å^3/atom)	$\Delta\Omega$ (%)	E_{tot} (eV/atom)	ΔH (eV/atom)	E_g (eV)
C54A	13.075	−10.1	−5.4728	−0.399	0.511/0.290
C54M	13.108	−9.8	−5.4579	−0.384	0.207/0.000
$C11_bA$	12.981	−10.7	−5.4713	−0.397	0.068/0.000
$C11_bM$	13.070	−10.1	−5.4417	−0.367	—
$C11_bM_{fm}$	13.136	−9.6	−5.4677	−0.393	—

investigated are listed in table 1. The total energy of Al_4MnCo in the C54A structure is $E_{tot}(\mathrm{C54A}) = -5.4737$ eV/atom.

The second structural variant of the Al_4MnCo compound is also derived from the C54 structure of Al_2Fe, where Mn and Co atoms replace Fe sites. In this case all pseudohexagonal TM–Al_2 layers have mixed Mn–Co occupancies. Figure 3 shows the DOS of Al_4MnCo in the C54M structure. The band gap at the Fermi level is much narrower. Analysis of the geometry and atomic position of the relaxed structure reveals a substantial distortion of the unit cell and large deviations of the atomic positions from their ideal sites. The pseudohexagonal plane becomes slightly puckered. The total energy of this structural variant, $E_{tot}(\mathrm{C54M}) = -5.4579$ eV/atom, is 15.8 meV higher in comparison with the variant with layers of alternating occupation (see table 2).

These values of total energies can be compared with the total energies of the pure elements in their ground-state structures: the total energy of Al in the fcc (A1) structure is $E_{tot}(\mathrm{A1}) = -3.6933$ eV/atom. The total energy of Mn in the hcp (A3) structure is $E_{tot}(\mathrm{A3}) = -8.884$ eV/atom. The total energy of Co in the hcp (A3) structure is $E_{tot}(\mathrm{A3}) = -6.8073$ eV/atom. A linear interpolation of these values for the Al_4MnCo composition gives −5.0589 eV/atom, leading to a heat of formation of the C54A structure $\Delta H = -0.399$ eV/atom. Heats of formation for all structures investigated are listed in tables 1–3.

Our calculations suggest that Al_4MnCo in the C54A or C54M structures is an intermetallic semiconductor. The real existence of such a compound depends on the possible existence of other compounds of the same or similar composition. Compounds derived from the $C11_b$ structure are certainly such candidates.

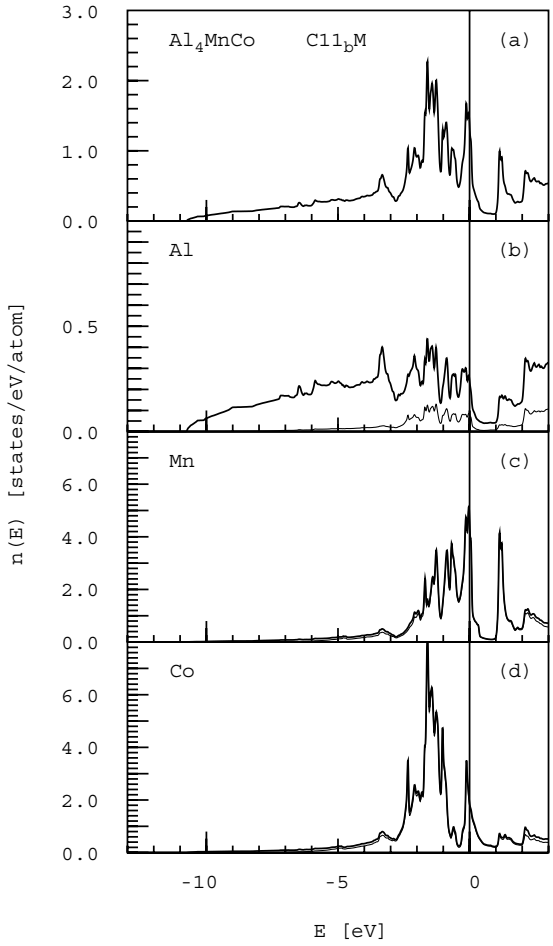

Figure 4. The densities of states of the Al_4MnCo compound in the $C11_bM$ structure. The figure presents the total DOS (a), partial aluminium DOS (b), partial TM DOSs for Mn (c) and Co (d) atoms. The thin line indicates the d-state contribution. A clear difference from the results for the C54A structure is seen—the band gap is missing.

Table 3. Equilibrium volume Ω, excess volume $\Delta\Omega$, total energy E_{tot}, heat of formation ΔH, and width of the gap at the Fermi level E_g of Al_4ReIr for several lattice types.

Al_4ReIr in lattice	Ω (Å^3/atom)	$\Delta\Omega$ (%)	E_{tot} (eV/atom)	ΔH (eV/atom)	E_g (eV)
C54A	14.373	−9.8	−6.5924	−0.627	1.019/0.698
$C11_bA$	14.325	−10.1	−6.5620	−0.597	0.149/0.042
$C11_bM$	14.466	−9.2	−6.5078	−0.543	—

3.1.2. The $C11_b$ structure. Figure 4 shows the total and partial Al, Mn, and Co densities of states of the Al_4MnCo compound in the $C11_bM$ structure. A clear difference from the previously discussed results for the C54A structure is seen immediately—the band gap is missing. The Fermi level is located close to the top of a high peak of the DOS. Decomposition of the DOS into partial contributions shows that the d states of the Mn atom give the main contribution to the height of this peak. The peak is followed by a deep pseudogap extending

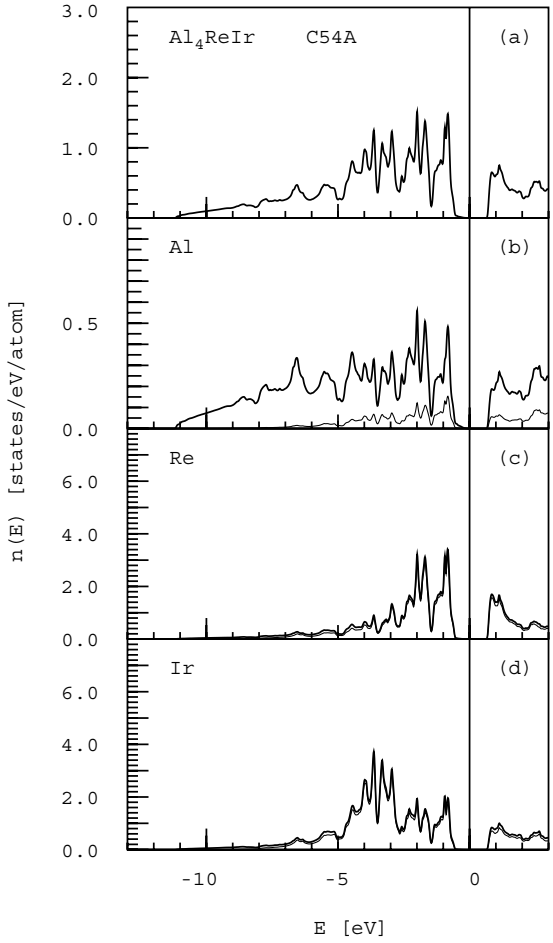

Figure 5. The DOS of the Al_4ReIr compound in the C54A structure. The figure presents the total DOS (a), partial aluminium DOS (b), partial TM DOSs for Re (c) and Ir (d) atoms. The thin line indicates the d-state contribution. The width of the semiconducting gap at the Fermi level $E_g \approx 1.0$ eV is reduced by a tail of the Al DOS extending from the valence band.

from 0.3 to 1.0 eV above the Fermi level. This pseudogap is repeated also in the partial Al and Mn densities. In the partial Co DOS one can see also a rather deep DOS minimum at energies around -0.35 eV below the Fermi level. The origin of both pseudogaps will become more clear from COOP analysis in section 5.1.

A high DOS at the Fermi level of the Mn atoms indicates a possible magnetic instability of Mn ions. We repeated the calculation for the Al_4MnCo compound in the $C11_bM$ structure in a spin-polarized state. The geometry of the cell and the internal structural parameters were also optimized in the spin-polarized state. Spin polarization is not negligible. In the spin-polarized state the Fermi level is located in the minimum of the majority band. We note that the existence of a true gap at the Fermi level that we have seen in the DOSs of the C54 structures forbids the existence of magnetic polarization in these structures.

The structural data and the total energy obtained by VASP calculations for both paramagnetic and spin-polarized states are given in table 2. The total energy of the Al_4MnCo

compound in the paramagnetic state, $E_{tot}(\mathrm{C11_bM}) = -5.4417$ eV/atom, is 31 meV higher than that of the C54A structure; in the ferromagnetic state the structural energy difference is reduced to 5 meV. Ferromagnetic ordering also induces a slight volume expansion.

This result is interesting to compare with the different total energies obtained [9] for the same structures in the case of Al_2Fe. In contrast to the case for the ternary compound, in the binary compound the $C11_b$ structure is more stable than the C54 structure (by about 21 meV). Although relaxation of the structure in the spin-polarized state substantially reduces the total energy, its value $E_{tot}(\mathrm{C11_bM_{fm}}) = -5.4677$ eV/atom is still 5 meV higher than that of the C54A structure.

We have calculated also the total DOS of Al_4MnCo compound in the $C11_bA$ structure. This structure consists of alternating pseudohexagonal Mn–Al_2 and Co–Al_2 layers. The electronic structure of this variant resembles that of Al_2Fe in the $C11_b$ structure. In comparison with figure 2, the band gap here shrinks almost to zero. The total energy of this structural variant is $E_{tot}(\mathrm{C11_bA}) = -5.4713$ eV/atom. The difference with respect to the total energy of the C54A structure is only 1.5 meV.

3.2. Electronic density of states of Al_4ReIr

The Al_4ReIr compound in the C54A structure exhibits the widest band gap. Figure 5 shows the total and the partial Al, Re, and Ir densities of states. The width of the gap at the Fermi level is $E_g \approx 1.0$ eV. If we neglect the tail of Al states extending from the lower-energy band edge, the width of the gap would be even wider, $E_g \approx 1.4$ eV.

The electronic structure of the Al_4ReIr compound in the $C11_bM$ structure exhibits a similar character to the electronic structure of Al_4MnCo in the $C11_bM$ structure seen in figure 4. The band gap is missing; the Fermi level is located in a region of high DOS. Above the Fermi level, a broad pseudogap extends up to $\sim$2 eV. The structural data and the total energies obtained by VASP calculations for both structures are listed in table 3. The C54A structure is found to be lowest in energy: about 30 meV/atom below the $C11_bA$ lattice.

4. Charge density distribution

Using the VASP program, we calculated the charge density distribution of Al_4MnCo in the elementary cell of the C54 and $C11_b$ structures. To study a possible covalent bonding, we investigated the electron density difference, i.e. a superposition of atomic charge densities is subtracted from the total charge density. We shall present in this paper only results for the C54A and $C11_bM$ structural variants for which, as we have seen, the characters of the DOSs significantly differ. As the bonding in the $C11_bM$ structure has appeared to be simpler than that in the C54A structure, we start first by discussing the results obtained for the $C11_bM$ structure.

4.1. Charge density distribution in the $C11_bM$ structure

Figure 6 shows a contour plot of the valence-charge difference distribution in the (001) plane (a) and the (002) plane (b) of the $C11_bM$ structure. The positions of the Mn and Co atoms are marked by filled circles. To facilitate the analysis, a schematic sketch of the tetragonal unit cell is shown in figure 7, highlighting the environment of the central Co atom. Mn atoms have a similar environment. The contour plot represents the regions of positive electron density difference in the (001) plane; in the blank areas the density difference is negative. If the character of the bonding is purely metallic, the charge distribution in the interstitial space should be homogeneous; a possible covalent bonding is indicated by enhanced charge

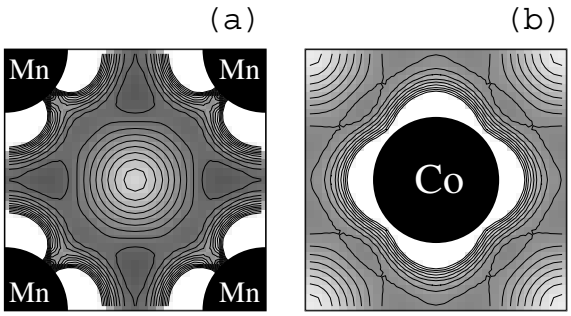

Figure 6. A contour plot of the valence-charge difference distribution in the (001) plane (a) and the (002) plane (b) of the Al_4MnCo in the $C11_bM$ structure. The positions of the Mn and Co atoms are marked by filled circles. The contour plot represents the regions of positive electron density difference; in the blank areas the density difference is negative. A possible covalent bonding is indicated by enhanced charge distribution along connections between atoms.

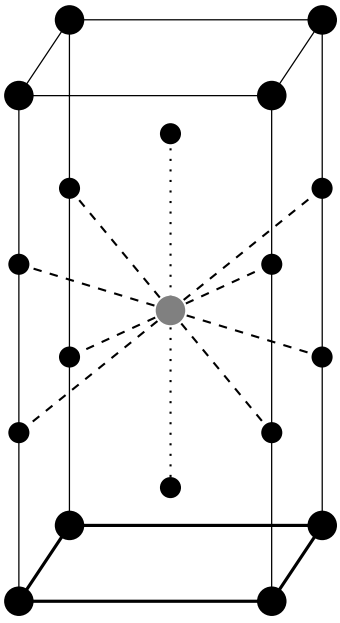

Figure 7. A schematic sketch of the tetragonal unit cell of the Al_4MnCo in the $C11_bM$ structure. Large circles: TM atoms; smaller circles: Al atoms. The bonding of the central Co atom with Al atoms is highlighted. The two different types of Co–Al bond are marked by dashed and dotted lines, respectively. Mn atoms have a similar environment. The Mn–Mn bonds in the tetragonal (001) plane are marked by thicker full lines.

distribution along connections between atoms. In figure 6 we see regions of enhanced charge density halfway between the Mn or Co atoms.

The pseudohexagonal plane in the $C11_bM$ structure is identical with the (110) plane. Figure 8 shows a contour plot of the valence-charge difference distribution in the (110) plane. The contour plot represents the regions of positive electron density difference; in the blank areas the density difference is negative. The positions of the Mn and Co atoms are marked by filled circles; the positions of the Al atoms are marked by open circles. An enhanced charge

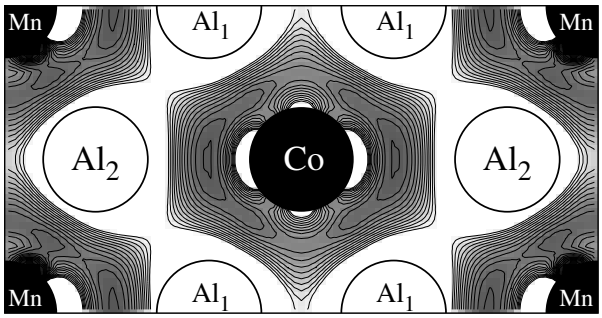

Figure 8. A contour plot of the valence-charge difference distribution in the (110) plane of the Al_4MnCo in the $C11_bM$ structure. The contour plot represents the regions of positive electron density difference; in the blank areas the density difference is negative. The positions of the Mn and Co atoms are marked by filled circles; the positions of the Al atoms are marked by open circles. An enhanced charge density is seen along the z-direction (horizontal) between the central Co atom and two Al_2 atoms. If the unit cell is periodically repeated, the same picture would be seen also for bonding charge between Mn and two Al_1. There are also enhanced charge densities between the Mn atoms in the corners of the unit cell and the Al_2 atoms. Somewhat weaker bonding is seen between the Co and four neighbouring Al_1 atoms.

density is seen along the z-direction between the central Co atom and the two Al_2 atoms. If the unit cell is periodically repeated, the same picture would be seen also for bonding charge between Mn and two Al_1. There are also enhanced charge densities between the Mn atoms in the corners of the unit cell and the Al_2 atoms. Somewhat weaker bonding is seen between the Co and four neighbouring Al_1 atoms. Due to the elongated shape of the unit cell, the hexagonal symmetry of the charge distribution is broken. The four Al_1 atoms in the (110) plane together with the other four equivalent Al_1 atoms from the perpendicular $(0\bar{1}1)$ plane form a distorted cubic coordination shell around the central Co atom. Mn atoms have the same cubic coordination, formed by Al_2 atoms.

In summary, there are possibly covalent bonds of several types: in the tetragonal (001) or (002) planes, TM atoms are bonded to four neighbouring TM atoms located on the corners of a square. As d orbitals always have inversion symmetry, bonds of TM with Al atoms occur in pairs of Al atoms in opposite directions. There are two types of bond between TM and Al atoms. One is directed along the z-axis; four bonds are oriented along body diagonals of the cube. The character of the bonds is investigated further in section 5.1.

4.2. Charge density distribution in the C54A structure

In the C54A structure, (001) and (004) pseudohexagonal planes have Mn–Al_2 and Co–Al_2 occupancy, respectively. The charge distribution in these planes is similar to that in Al_2Fe in the C54 structure studied in our recent paper [9]. In both (001) and (004) planes there is bonding of the central TM atom with the neighbouring six Al atoms. However, while bonding of Mn atoms is stronger with two Al atoms arranged together with the Mn atom along the x-direction and weaker with four other Al atoms in the pseudohexagonal plane, for the Co atoms the bonding situation is just the opposite.

TM atoms have ten aluminium neighbours. Six Al atoms are in the pseudohexagonal plane discussed above; the remaining four neighbours can be found in (011) and $(0\bar{1}1)$ planes. Figure 9 shows a contour plot of the valence-charge difference distribution in the (011) plane. As the (011) and $(0\bar{1}1)$ planes are related by a pseudo-S_6 symmetry around the x-axis, the

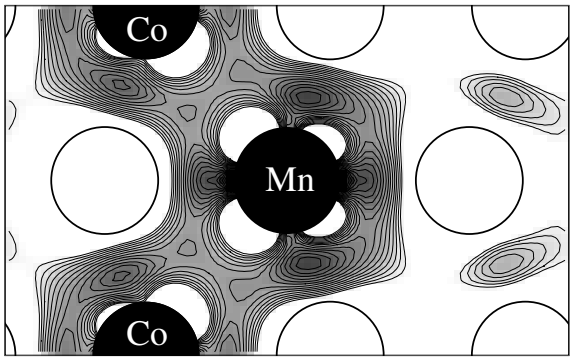

Figure 9. A contour plot of the valence-charge difference distribution in the (011) plane of the Al_4MnCo in the C54A structure. The positions of the Mn and Co atoms are marked by filled circles; the positions of the Al atoms are marked by open circles. The contour plot represents the regions of positive electron density difference; in the blank areas the density difference is negative. In the (011) plane we see regions of enhanced charge density halfway between the central Mn atoms and the Al neighbours. Bonding of the Co atom with the Al neighbours is also clearly recognizable. In addition, there are enhanced charge distributions between pairs of Al neighbours seen on the right in the figure. As the (011) and $(0\bar{1}1)$ planes are related by a pseudo-S_6 symmetry around the x-axis, $(0\bar{1}1)$ planes exhibit a similar charge distribution.

$(0\bar{1}1)$ plane exhibits a similar charge distribution. In the (011) plane in figure 9 we see regions of enhanced charge density halfway between the central Mn atom and the Al neighbours. The bonding of a Co atom with its Al neighbours is somewhat weaker, but still clearly recognizable. In addition, we clearly see enhanced charge distribution between pairs of Al neighbours.

In summary, also in this case there are possibly covalent bonds of several types. In the pseudohexagonal planes the TM atom is bonded with two Al atoms located on both sides of the TM atom along the x-axis. These two bonds differ from the other four bonds with the remaining four Al atoms in the pseudohexagonal plane. In the (011) plane we see two bonds along the x-axis with the same Al atoms as in the pseudohexagonal (001) plane and two bonds with other Al atoms, forming Al–TM–Al with a bond angle $\approx 149°$. These two Al atoms with the corresponding other two atoms from $(0\bar{1}1)$ plane form a distorted tetrahedral coordination around the TM atom in the centre. The character of the bonds is investigated in the next section.

5. Hybridized orbitals and covalent bonding

To gain a deeper understanding of the bonds identified in the density contour plots, we attempted to construct sets of symmetrized hybridized orbitals oriented along the bonds and calculated the DOS projected onto bonding and antibonding combinations of these symmetrized orbitals. The difference (B − A) between bonding (B) and antibonding (A) projected densities is essentially equivalent to the differential COOP defined by Hoffmann [10]. The symmetrized orbitals are sets of hybridized orbitals possessing the point group symmetry of a particular atomic site. A set of bonds originating from a particular atom forms a reducible representation of the point group. Decomposition of the reducible representation into irreducible ones enables one to select individual s, p, or d orbitals whose linear combinations form the hybridized orbitals.

5.1. Hybridized orbitals and covalent bonding in the $C11_bM$ structure

Similarly to in our recent study of bonding in Al_3V in the DO_{22} structure [17], the symmetry of $C11_bM$ is tetragonal. The point group symmetry of the TM sites is D_{4h}. The orbitals directed from the central TM atom to the eight Al atoms at the vertices of a tetragonal prism (almost a cube) and to the two other Al atoms located along the z-axis form the basis of a reducible representation of the D_{4h} point group. From its decomposition into the irreducible representations [9], we have found that the sd^3 hybrid orbitals formed by s, $d_{x^2-y^2}$, d_{zx}, d_{yz} states dominate the bonding. The d_{z^2} orbital apparently participates in bonding with two Al atoms located on the z-axis. It is remarkable that the symmetry here excludes the $d_{x^2-y^2}$ orbital from bonding. This is in turn the orbital which plays the dominant role in the TM–TM bonding in the tetragonal (001) and (002) planes. The symmetrized sd^3 orbitals have a form similar to that of the d_{z^2} orbital and differ only in orientation. While the d_{z^2} orbital is oriented along the z-axis, the symmetrized sd^3 orbitals are oriented along the body diagonals of a cube.

Figure 10 shows the differential COOP, for:

(a) bonding of Mn $d_{x^2-y^2}$ orbitals in the tetragonal (001) plane;
(b) bonding of Mn d_{z^2} orbitals with two sp hybridized orbitals on Al atoms; and
(c) bonding of an sd^3 hybridized orbital on a Mn atom with sp^3 d hybridized orbitals on Al atoms.

In the right-hand panel the configurations of bonding orbitals are displayed schematically. The corresponding COOP is presented in the left-hand panels. For each bonding configuration we see a clear bonding–antibonding splitting. The bonding–antibonding splitting of d orbitals is particularly strong for Mn–Mn bonding in the tetragonal (001) plane; see part (a) of figure 10. The bonding states at around -1.8 eV and the antibonding states extending between 1.0 and 1.5 eV are separated by a gap of $\approx$2.0 eV width. The Fermi level is here approximately in the middle of the gap. In the COOP of the Mn atom with Al atoms presented in parts (b) and (c), a separation of bonding and antibonding states by a gap is also clearly seen. However, in this case the gap is located above the Fermi level. In case (b) the gap extends from 0.3 to 1.2 eV and in case (c) from 0.5 to 1.3 eV (or even to 2.5 eV provided that we neglect a small bonding contribution seen in the figure at energies of 1.3–2.5 eV). The gaps seen in the COOPs for the three bonding configurations overlap only in the interval (0.3, 1.0) eV. The bonding or antibonding peaks in the COOP clearly coincide with peaks in the partial Mn DOS presented in figure 4. We also see that the peak at the Fermi level in the partial Mn DOS apparently has bonding character; cf figure 10(c).

The bonding situation for Co atoms in the $C11_bM$ structure is quite different. Figure 11 shows the differential COOP:

(a) for Co–Co bonding via Co $d_{x^2-y^2}$ orbitals in the tetragonal (002) plane;
(b) for bonding of Co d_{z^2} orbitals with two sp hybridized orbitals on Al atoms; and
(c) for bonding of sd^3 hybridized orbitals on the Co atom with two sp^3 d hybridized orbitals on Al atoms.

In the right-hand panel the configurations of bonding orbitals are displayed schematically. Although both the Co–Co and Co–Al COOPs presented in figures 11(a) and (b) exhibit bonding–antibonding splitting, no common band gaps exist. The gaps between bonding and antibonding states for configurations (a) and (b) extend below the Fermi level at energies from ≈ -1.0 to -0.7 eV. On the other hand, the bonding configuration presented in figure 11(c) exhibits a wide gap extending above the Fermi level from 0.05 to 1.3 eV. Comparison of the peaks observed in the COOP with the partial Co DOS presented in figure 4(d) helps one to

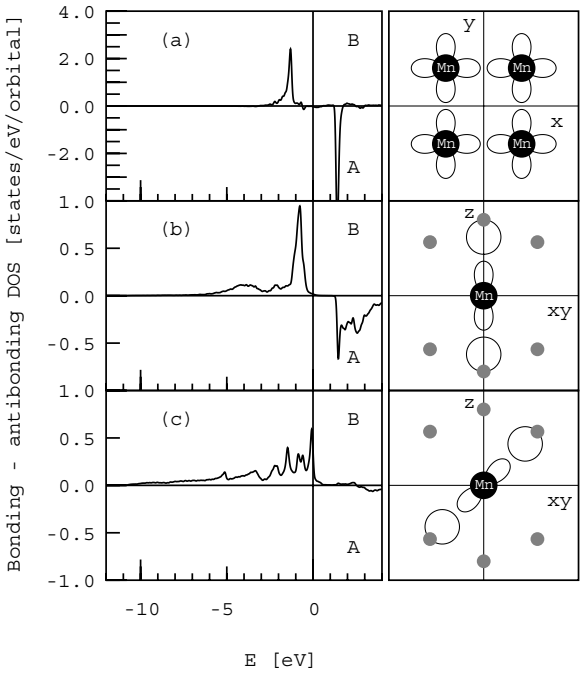

Figure 10. A COOP of Al_4MnCo in the $C11_bM$ structure for (a) bonding of Mn $d_{x^2-y^2}$ orbitals in the tetragonal (001) plane, (b) bonding of Mn d_{z^2} orbitals with two sp hybridized orbitals on Al atoms, and (c) bonding of the sd^3 hybridized orbital on the Mn atom with sp^3 d hybridized orbitals on Al atoms. In the right-hand panel the configurations of bonding orbitals are displayed schematically. The corresponding COOP is presented in the left-hand panels. For each bonding configuration we see a clear bonding–antibonding splitting of states. Groups of bonding and antibonding states are separated by a gap.

understand the character of the peaks and minima in the partial DOS. The peak at the Fermi level in the Co DOS apparently has antibonding character and the pseudogap below this peak comes from the bonding configurations shown in figures 11(a) and (b).

5.2. Hybridized orbitals and covalent bonding in the C54A structure

A detailed analysis of hybridized orbitals and covalent bonding in the C54A structure in Al_2Fe and related TM compounds has already been performed in our previous paper [9]. The DOS and charge density analysed in sections 3.1.1 and 4.2 have demonstrated close similarities to those observed for Al_2Fe, so we can expect a similar picture of bonding also from the COOP analysis.

The point group symmetry of C54A is D_{2h}, i.e. it is rather low. The symmetry does not split any group of orbitals; neither does it exclude any orbital from the bonding. A clean gap in the band structure hence indicates that if the bonding has covalent character and the gap originates from the bonding–antibonding splitting, then all orbitals must participate in the bonding. The molecular orbitals corresponding to the bonding and antibonding states include all orbitals in the system. The configuration of the Al orbitals participating in the bonding is quite simple. As each Al atom has in the pseudohexagonal planes three TM neighbours located at the vertices of a triangle, the symmetrized orbitals correspond to sp^2 hybridization. The symmetrized orbitals are constructed as a linear combination of s, p_x, and p_y orbitals.

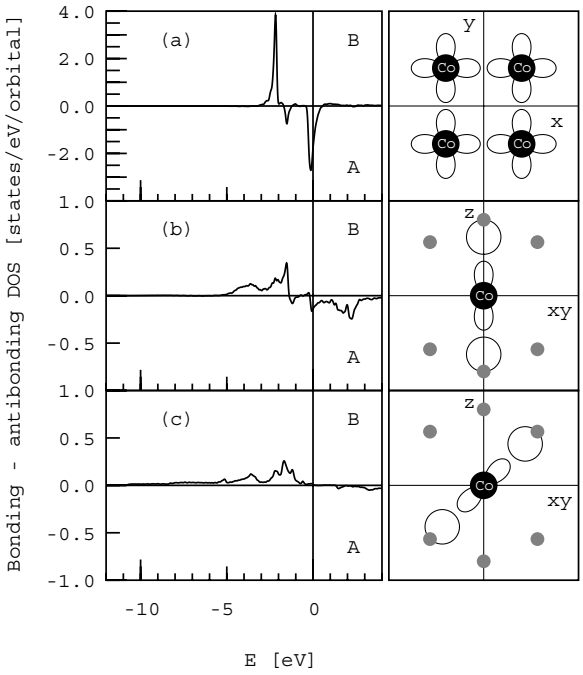

Figure 11. A COOP of Al_4MnCo in the $C11_bM$ structure for (a) Co–Co bonding of Co $d_{x^2-y^2}$ orbitals in the tetragonal (002) plane, (b) bonding of Co d_{z^2} orbitals with two sp hybridized orbitals on Al atoms, and (c) bonding of the sd^3 hybridized orbital on the Co atom with two sp^3 d hybridized orbitals on Al atoms. In the right-hand panel the configurations of bonding orbitals are displayed schematically. Although both the Co–Co and Co–Al bonding configurations presented in (a) and (b) exhibit bonding–antibonding splitting, the groups of bonding and antibonding states are separated by a gap less clearly. The gaps are partially covered by some residual states.

The remaining p_z orbital participates in the bonding between neighbouring pseudohexagonal planes.

The participation of Mn or Co d orbitals in the bonding is more complex. Let us consider first the bonding of Mn atoms. Figure 12 presents the COOP of typical bonding configurations. Part (a) shows the bonding around a Mn atom in the pseudohexagonal (001) plane. Hybridized d^2 orbitals (combinations of d_{xy} and $d_{x^2-y^2}$ orbitals) interact with two sp^2 hybridized orbitals on Al atoms. The corresponding COOP shows a clear splitting of bonding and antibonding states with a gap of $\approx$0.7 eV. The COOP changes sign just at the Fermi level.

The interplanar bonding in the C54 structure is quite complex. We present bonding configurations corresponding to the strong charge enhancement in the (011) plane shown in figure 9 only. The d^5 hybridized orbital on the Mn atom oriented towards the Al atom includes all five d orbitals. From the Al side we have only the p_z orbital oriented along the z-axis. The orientation of the bonding orbitals is here not coaxial. To explain this bonding situation we make two remarks. Although in this picture p_z does not have the maximal overlap with the orbital centred at the Mn atom, we should keep in mind that d orbitals on the Al atom that we have not considered so far hybridize with the p_z orbital and improve the overlap. Secondly, as we shall see below, the same p_z orbital participates also in the Al–Al bonding and overlaps with the p_z orbital from the other Al atom. The gap between the bonding and antibonding states seen in the COOP in figure 12(b) extends over the same energy range as the gap in the in-plane bonding configuration discussed in part (a). Figure 12(c) shows the

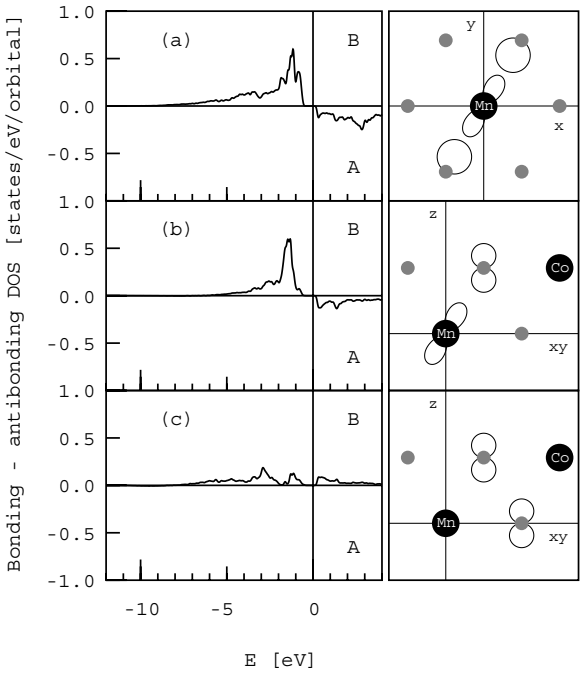

Figure 12. A COOP of typical bonding configurations (right-hand panel) of Al_4MnCo in the C54A structure of the Mn atom in the C54A structure. The corresponding COOPs are in the left-hand panels. Part (a) shows the bonding of the Mn atom in the pseudohexagonal (001) plane. The hybridized d^2 orbital interacts with two sp^2 hybridized orbitals on Al atoms. The COOP shows a clear splitting of bonding and antibonding states separated by a gap of $\approx$0.7 eV width. Part (b) shows the COOP for interplanar Mn–Al bonding. The d^5 hybridized orbital on the Mn atom is oriented towards the Al atom. From the Al side there is a p_z orbital oriented along the z-axis. The bonding of the Co atom in the pseudohexagonal (004) plane is very similar to the bonding of the Mn atom in the (001) plane. Part (c) represents a bonding situation for two Al atoms in the (011) plane. The bond is formed by two overlapping p_z orbitals located on both Al atoms. Contrary to all previous results, the COOP here is simultaneously positive below and above the Fermi level.

bonding configuration and the corresponding COOP for Al–Al bonds seen in figure 9. The bond is formed by two overlapping p_z orbitals located on both Al atoms. Contrary to all previous results, the COOP here is simultaneously positive below and above the Fermi level. This also indicates covalent bonding, but the Al–Al bond is here not fully populated and the bonding–antibonding splitting occurs at higher energies. The missing states around the Fermi level were absorbed in hybridized orbitals participating in other Al–TM bonds.

The COOP analysis of bonding around the Co atom shows that there is not too much difference from the case of the Mn atom. Again we see that there is a clear bonding–antibonding splitting in the COOPs for both in-plane and interplane bonding mediated by the Co atom. The important point is that the gaps between the bonding and antibonding states not only have almost the same width and the same position for different kinds of Co bond, but also coincide with the gaps seen in the Mn COOPs. In this respect the situation is very different from the case for the $C11_bM$ structure discussed in the previous subsection.

We make several concluding remarks:

(i) The results for the COOP prove that in Al_4MnCo with C54A structure there are covalent bonds between Al and TM atoms and partially also between Al and Al atoms. There is no significant bonding between TM atoms.

(ii) The gap in the electronic band has the character of bonding–antibonding splitting of the electronic states.

6. Summary and conclusions

In this paper we have extended our previous study of the electronic structure and bonding mechanism in TM di-aluminides to ternary systems. We have restricted our study to the layered structures C54 ($TiSi_2$) and $C11_b$ ($MoSi_2$) in which the TM di-aluminides exhibit semiconducting behaviour. In our previous study we have seen that a semiconducting band gap exists in Al_2TM compounds where TM atoms have eight valence electrons. The semiconducting gap does not disappear if TM sites are occupied by two different TMs, TM_1 and TM_2, provided that the electron-per-atom ratio is conserved. Such a replacement substantially increases the class of possibly semiconducting TM di-aluminides. We calculated the electronic structure for nine $Al_4TM_1TM_2$ compounds by combining early and late TMs from the 3d, 4d, and 5d rows of the periodic table. We presented here the results for the compounds with TM sites occupied by TM atoms from the same row of the periodic table only, but the semiconducting gap is present also in the compounds with TM sites occupied by atoms from different rows of the periodic table. A substitution with 3d TM atoms for 4d or 5d metals enhances the width of the gap. We have performed a detailed study of the electronic structure for the Al_4MnCo compound that we consider representative for this class of intermetallics.

From the analysis of the charge density distribution and the COOP we have found that the bonding between atoms has dominantly covalent character. This is seen not only from the enhanced charge density halfway between atoms, but also from the clear bonding–antibonding splitting of the electronic states. In a particular bonding configuration, groups of bonding and antibonding states are separated by a gap. If the gaps between groups of bonding and antibonding states that correspond to all bonding configurations in the unit cell have a common overlap, then the semiconducting band gap in the DOS can be formed.

Results of the total-energy calculations suggest that the existence of a band gap does not necessarily mean a stable structure. Strong covalent bonds can exist also in structures where no band gap is observed. The total energy of Al_4MnCo has been found to be the lowest for the C54A structure with a large semiconducting gap. However, the structural energy difference of only 5 meV with respect to the metallic $C11_bM$ structure is apparently not enough to maintain its semiconducting character up to room temperatures. The situation is different in the case of Al_4ReIr, where no significant contribution from magnetic interactions to stabilize the metallic $C11_bM$ structure can be expected. The most stable phase in this system is thus the C54A structure with the large semiconducting gap. Al_4ReIr is therefore the best candidate for being an intermetallic semiconductor. Other possible candidates are Al_4MoPd and Al_4WPt.

Although not all the phases studied necessarily exist as real experimentally observed phases, in thermodynamically excited metastable systems such as amorphous, nanocrystalline materials or quasicrystals, bonding configurations similar to those analysed here can exist. Our study can thus help with understanding the anomalous physical properties of these materials also. In particular, the high resistivities of icosahedral AlPdRe quasicrystalline samples could be explained by the existence of a narrow band gap in the spectrum at the Fermi level. We have already demonstrated the possibility of the existence of such a gap in our recent paper [18]. In the near future we intend to extend our study to such more complex systems.

Acknowledgments

This work was supported by the Austrian Ministry for Education, Culture and Science through the Centre for Computational Materials Science. MK also acknowledges support from the Grant Agency for Science in Slovakia (Grant no 2/2038/22).

References

[1] Inoue A, Kimura H, Sasamori K and Masumoto T 1996 *Mater. Trans. JIM* **37** 1287
[2] Stadnik Z M (ed) 1999 *Physical Properties of Quasicrystals (Springer Series in Solid-State Sciences vol 126)* (Berlin: Springer)
[3] Srinivas V, Rodmar M, Poon S J and Rapp Ö 2001 *Phys. Rev.* B **63** 172202
[4] Rapp Ö 1999 *Physical Properties of Quasicrystals (Springer Series in Solid-State Sciences vol 126)* ed Z M Stadnik (Berlin: Springer) p 127
[5] Weinert M and Watson R E 1998 *Phys. Rev.* B **58** 9732
[6] Nguyen Manh D, Trambly de Laissardière G, Julien J P, Mayou D and Cyrot-Lackmann F 1992 *Solid State Commun.* **82** 329
[7] Öğüt S and Rabe K 1996 *Phys. Rev.* B **54** R8297
[8] Springborg M and Fischer R 1998 *J. Phys.: Condens. Matter* **10** 701
[9] Krajčí M and Hafner J 2002 *J. Phys.: Condens. Matter* **14** 5755
[10] Hoffmann R 1988 *Solids and Surfaces: a Chemist's View of Bonding in Extended Structures* (New York: VCH)
[11] Pearson W B 1972 *The Crystal Chemistry and Physics of Metals and Alloys* (New York: Wiley)
[12] Kresse G and Furthmüller J 1996 *Comput. Mater. Sci.* **6** 15
Kresse G and Furthmüller J 1996 *Phys. Rev.* B **54** 11 160
[13] Kresse G and Joubert D 1999 *Phys. Rev.* B **59** 1758
[14] Andersen O K 1975 *Phys. Rev.* B **12** 3060
Skriver H L 1984 *The LMTO Method* (Berlin: Springer)
[15] Andersen O K, Jepsen O and Götzel D 1985 *Highlights of Condensed Matter Theory* ed F Fumi and M P Tosi (New York: North-Holland)
[16] Andersen O K, Jepsen D and Šob M 1987 *Electronic Band Structure and its Applications* ed M Youssouff (Berlin: Springer)
[17] Krajčí M and Hafner J 2002 *J. Phys.: Condens. Matter* **14** 1865
[18] Krajčí M and Hafner J 2001 *J. Phys.: Condens. Matter* **13** 3817